Desalination and Water Treatment
www.deswater.com
doi: 10.5004/dwt.2021.27318

228 (2021) 403–413
July

Conventional and ultrasound-assisted bioaccumulation of azo dye Indosol Black NF-1200 by kefir biomass

Hatice Mutlu, Dilek Kılıç Apar*

Chemical Engineering Department, Yıldız Technical University, Davutpaşa Campus, 34210 Istanbul, Turkey, Tel. +90 536 588 67 78; email: dkilic@yildiz.edu.tr (D. Kılıç Apar), Tel. +90 555 671 39 91; email: hatice.bgs@gmail.com (H. Mutlu)

Received 24 April 2020; Accepted 9 April 2021

ABSTRACT

In the present work, conventional and ultrasound-assisted bioaccumulation of direct azo dye Indosol Black NF-1200 (IB) by active kefir biomass was investigated. The kefir biomass was characterised by scanning electron microscopy, Fourier transform infrared spectroscopy and Brunauer–Emmett–Teller analyses. Batch mode experiments were carried out to study the effect of experimental factors such as pH, initial dye concentration and temperature on IB dye bioaccumulation. Both in conventional and ultrasound-assisted bioaccumulation the dye removal percentage increased with the decrease in pH and initial dye concentration and with the increase in temperature. Higher dye removal efficiencies were achieved, and the equilibrium times significantly decreased in bioaccumulation processes assisted by ultrasound. The enhancement effect of ultrasound was more significant at high pHs, high dye concentrations and low temperatures. Dye removals of 73% and 96% were obtained at pH 2, 25°C and 50 mg L^{-1} initial dye concentration for conventional and ultrasound-assisted bioaccumulation in which the equilibrium was reached within 180 and 30 min, respectively. The kinetic data fitted well with pseudo-first-order and pseudo-second-order kinetic models for conventional and ultrasound-assisted bioaccumulation, respectively. Equilibrium data of both processes fitted well with the Langmuir isotherm model. Ultrasound-assisted bioaccumulation of a dye was investigated for the first time in this study. The results reveal that ultrasound can be used as a powerful option for the improvement of bioaccumulation processes and showed that kefir biomass could be used effectively for the removal of direct dyes.

Keywords: Azo dye; Bioaccumulation; Kefir biomass; Modelling; Ultrasound

1. Introduction

Dyes are chemical compounds that are extensively used in the textile, leather, paper, pharmaceutical, food and cosmetic industries to colour products. They are extremely stable and difficult to degrade in nature as they are designed to withstand fading when subjected to water, heat, light and oxidizing agents [1–3]. Even in very small amounts (<1 ppm), the existence of synthetic dyes in water bodies is highly visible. The release of dye effluents into the environment is not solely a matter of concern for aesthetic reasons. It has been reported that many dyes and their degradation products are toxic, mutagenic or carcinogenic and thus harmful to human health and the environment [2,4,5].

Various physical, chemical and biological methods are available for the removal of dyes from effluents. Among them, adsorption is one of the most efficient because of the process yield, high selectivity and cost-effectiveness [6–8]. In recent years, much attention has been devoted to the investigation of low-cost, eco-friendly adsorbents derived from biological organisms and several fungi, algae, yeasts and bacteria have been reported as potential bioadsorbents for dye removal [9–12].

* Corresponding author.

Sonication has been widely used in the production stage of adsorbents and as a pre-treatment to increase the surface area and porosity of the adsorbents [13–15]. Also, ultrasound has been applied simultaneously with adsorption to enhance the process efficiency in numerous studies as ultrasonic radiation leads to acceleration in reaction and mass transfer rates because of the acoustic cavitation that covers the creation, growth, and collapse of microbubbles [16–19].

Kefir grains are small, irregularly shaped white or yellow masses that consist of various lactic acid bacteria, acetic acid bacteria and yeasts that are used as starter cultures in the fermentation of milk to produce probiotic kefir drinks [20,21]. Kefir grains (kefir biomass) were used in reactive dye removal for the first time in a recent study by Erdoğdular and Apar [22]. The results of that study indicate that kefir biomass has great potential as an economical, eco-friendly and reusable bioadsorbent for reactive dyes. Consequently, in the present work, we aimed to investigate the effectiveness of active kefir biomass in the removal of a direct azo dye (Indosol Black NF-1200) and the enhancement of the dye removal efficiency of the biomass with the assistance of ultrasound. The present work is the first study in the literature in which the bioaccumulation of a dye under sonication is investigated.

2. Materials and methods

2.1. Dyestuff

Direct azo dye Indosol Black NF-1200 (Direct Black 22) was supplied by Clariant Co., (Kocaeli, Turkey). The molecular structure and properties of the Indosol Black NF-1200 dye are shown in Table 1.

2.2. Kefir grains and propagation

The starter culture of kefir grains was supplied by Ege University, Dairy Technology Department (Izmir, Turkey). Kefir grains were cultured in whey solution to increase the kefir biomass. The whey solution was prepared to contain 5% lactose (since the milk that is the natural culturing medium for kefir grains consists of 5% lactose) by dissolving whey powder in distilled water. Whey powder was supplied by Maybi Co., (Tekirdağ, Turkey). Throughout the study, the culture medium was refreshed daily.

2.3. Characterisation of kefir biomass

The isoelectric point of kefir grains was determined by measuring the zeta potentials of the samples at various pHs using a Zetasizer (Malvern Nano ZS MPT2). The surface morphology of the biomass samples was examined with a scanning electron microscope (Zeiss EVO LS 10). Fourier transform infrared spectroscopy (FTIR) analyses were carried out using Fourier transform infrared spectroscopy (PerkinElmer Spectrum 100). The surface area and the pore size distribution of the samples were determined by the N_2 adsorption–desorption method using a Brunauer–Emmett–Teller surface analyser (Quantachrome – Quadrasorb SI). Adsorption–desorption isotherms were measured at 77 K. To remove moisture content on the sample surface, all samples were degassed at 40°C for 12 h before analysis.

Before all analyses, kefir samples were dried at 45°C for 24 h.

2.4. Bioaccumulation experiments

Conventional and ultrasound-assisted bioaccumulation experiments were conducted simultaneously in batch mode to investigate the effects of different parameters such as initial pH (2–10), temperature (25°C–40°C) and initial dye concentration (50–400 mg L^{-1}) on Indosol Black NF-1200 (IB) dye bioaccumulation. The effects of all these parameters on dye bioaccumulation were investigated regarding time. For each pair of experiments (ultrasound-assisted and conventional), 100 mL of dye solutions at certain concentrations (100 mg L^{-1} for pH and temperature experiments and 50, 100, 200, 300 and 400 mg L^{-1} for initial dye concentration experiments) were taken in 250 mL Erlenmeyer flasks. The pH values of the solutions were adjusted (by 0.5 M HCl and 0.5 M NaOH solutions), heated to the desired temperature and then the dye removal processes were begun with the addition of kefir biomass. During treatments, one of the flasks was kept in a temperature-controlled shaker (IKA, KS 4000i) and the other in an ultrasonic bath (Alex-Machine). The temperature of the ultrasonic bath was monitored using a digital thermocouple and kept constant by circulating ethylene glycol-water solution within a coil immersed in the bath. Throughout the experiments, samples were taken from the solutions at specified times to determine the dye concentration.

Table 1
Molecular structure and properties of Indosol Black NF-1200

Name	Molecular structure
Indosol Black NF-1200, Direct Black 22, C.I. Direct Black, C.I. 35435	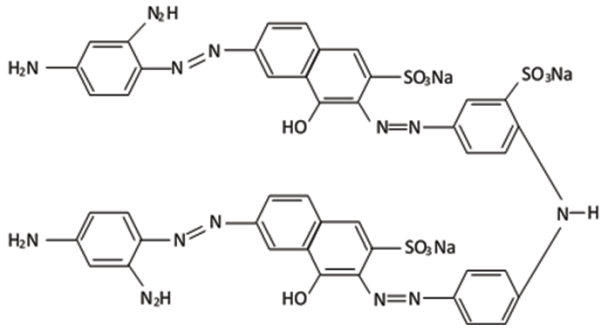
Molecular formula $C_{44}H_{32}N_{13}Na_3O_{11}S_3$	
Molecular weight 1,083.87 g mol^{-1}	

Sample absorbances were measured at 492 nm (λ_{max} of IB dye) using a UV-Vis spectrophotometer (Analytik Jena SPECORD 200) and converted to the concentration values using the constructed calibration curve for the dye.

Dye removal percentage and the bioaccumulation capacity (q_t, mg g^{-1}) were calculated according to Eqs. (1) and (2):

$$\text{Dye Removal\%} = \frac{C_0 - C_t}{C_0} \times 100 \quad (1)$$

$$q_t = \frac{V\left(C_0 - C_t\right)}{M} \quad (2)$$

In Eqs. (1) and (2), C_0 (mg L^{-1}) is the initial dye concentration, C_t (mg L^{-1}) is the dye concentration at the processing time t (min), V (L) is the solution volume and M (g) is the dry weight of the kefir biomass.

2.5. Bioaccumulation kinetics

Kinetic data were analysed using pseudo-first-order [Eq. (3)], pseudo-second-order [Eq. (4)], intraparticle diffusion [Eq. (5)] and Elovich [Eq. (6)] kinetic models to investigate the mechanism of bioaccumulation processes.

$$\ln\left(q_e - q_t\right) = \ln q_e - k_1 t \quad (3)$$

$$\frac{t}{q_t} = \frac{1}{k_2 q_e^2} + \frac{1}{q_e} t \quad (4)$$

$$q_t = k_p t^{1/2} + C \quad (5)$$

$$q_t = \frac{1}{\beta}\ln\left(\alpha\beta\right) + \frac{1}{\beta}\ln t \quad (6)$$

In Eqs. (3)–(6), q_e (mg g^{-1}) and q_t (mg g^{-1}) are the adsorbed dye amounts per unit mass of kefir biomass at equilibrium and at time t (min), k_1 (min^{-1}), k_2 (g mg^{-1} min^{-1}) and k_p (mg g^{-1} min$^{-1/2}$) are pseudo-first-order, pseudo-second-order and intraparticle diffusion rate constants, C (mg g^{-1}) is intraparticle diffusion model constant, α (mg g^{-1} min^{-1}) is the initial rate of adsorption, and β (g mg^{-1}) is desorption constant.

2.6. Equilibrium modelling

The equilibrium data were evaluated using Freundlich [Eq. (7)], Langmuir [Eq. (8)], and Temkin [Eq. (9)] isotherm models.

$$\ln q_e = \ln K_F + \frac{1}{n}\ln C_e \quad (7)$$

$$\frac{1}{q_e} = \frac{1}{q_m} + \left(\frac{1}{q_m K_L}\right)\frac{1}{C_e} \quad (8)$$

$$q_e = \frac{RT}{b_T}\ln K_T + \frac{RT}{b_T}\ln C_e \quad (9)$$

In Eqs. (7)–(9), q_e (mg g^{-1}) is adsorbed dye amount per unit mass of kefir biomass at equilibrium, q_m (mg g^{-1}) is maximum adsorption capacity, C_e (mg L^{-1}) is equilibrium dye concentration, and K_F (mg g^{-1} (mg L^{-1})$^{-1/n}$), K_L (L mg^{-1}), and K_T (L mg^{-1}) are Freundlich, Langmuir and Temkin constants, respectively, R (J mol^{-1} K^{-1}) is the gas constant, T (K) is temperature and b_T (J mol^{-1}) is the isotherm constant related to heat of adsorption.

3. Results and discussion

3.1. Kefir biomass characterisation

The isoelectric point or the point of zero charge (PZC) is the pH value for which the net surface charge of the adsorbent is zero. The PZC of the kefir biomass was determined as pH 4.46. This result suggests that at pHs < 4.46, the kefir biomass surface would be positively charged while at pHs > 4.46 the kefir biomass surface would be negatively charged.

Scanning electron microscopy (SEM) was used to illustrate the surface morphology of the kefir biomass before and after the bioaccumulation processes. Fig. 1a shows the morphology of the biomass before the bioaccumulation process. As seen from the micrograph, the surface of the kefir biomass is rough, uneven (typically asymmetrical) and highly porous. It is evident that the biomass contains many mesopores. The surface morphology of the biomass after ultrasound-assisted and conventional bioaccumulation processes is illustrated in Figs. 1b and c. As seen from these micrographs, the surface has become less rough since the dye molecules are diffused over pore cavities and cover the biomass surface.

FTIR analysis was performed to identify the functional groups present in the structure of kefir biomass before and after the bioaccumulation process. A FTIR spectrum was also obtained for the dye for comparison. All FTIR spectra are presented in Fig. 2. The kefir biomass showed characteristic peaks at 3,268; 2,923; 2,853; 1,630; 1,542; 1,413; 1,240; 1,118 and 871 cm^{-1}. The peak at 3,268 cm^{-1} is associated with the hydroxyl groups. The peaks at 2,923 and 2,853 cm^{-1} are indicative of C–H stretching vibrations. The peaks at 1,630 and 1,542 cm^{-1} are attributed to the C=O stretching that is characteristic of polysaccharides and the observed peaks at 1,413; 1,240 and 1,118 cm^{-1} are related to C–O–C and C–C stretching vibrations. The peak at 871 cm^{-1} is indicative of β-configuration and the vibration modes of glucose and galactose (Fig. 2a) [23–25]. The FTIR spectrum of the dye showed specific peaks at 3,330 cm^{-1} for O–H stretching, 2,925 cm^{-1} for aromatic C–H stretching, 1,590 cm^{-1} for N=N stretching vibrations and 1,470 cm^{-1} for aromatic ring stretching. The region between 1,354 and 706 cm^{-1} represents the characteristic bands of sulfonate groups (Fig. 2c) [26,27]. The FTIR spectrum of the kefir grains loaded with IB dye (Fig. 2b) displayed some changes caused by the adsorption of dye. The intensities of the peaks increased as a result of the interactions between the biomass functional groups and dye molecules. Also, the peaks at 3,268; 1,630; 1,542; 1,413 and 1,240 cm^{-1} shifted to 3,282; 1,637; 1,541; 1,375 and 1,235 cm^{-1}, respectively.

The N_2 adsorption isotherm and pore size distribution of kefir biomass and ultrasound treated kefir biomass samples

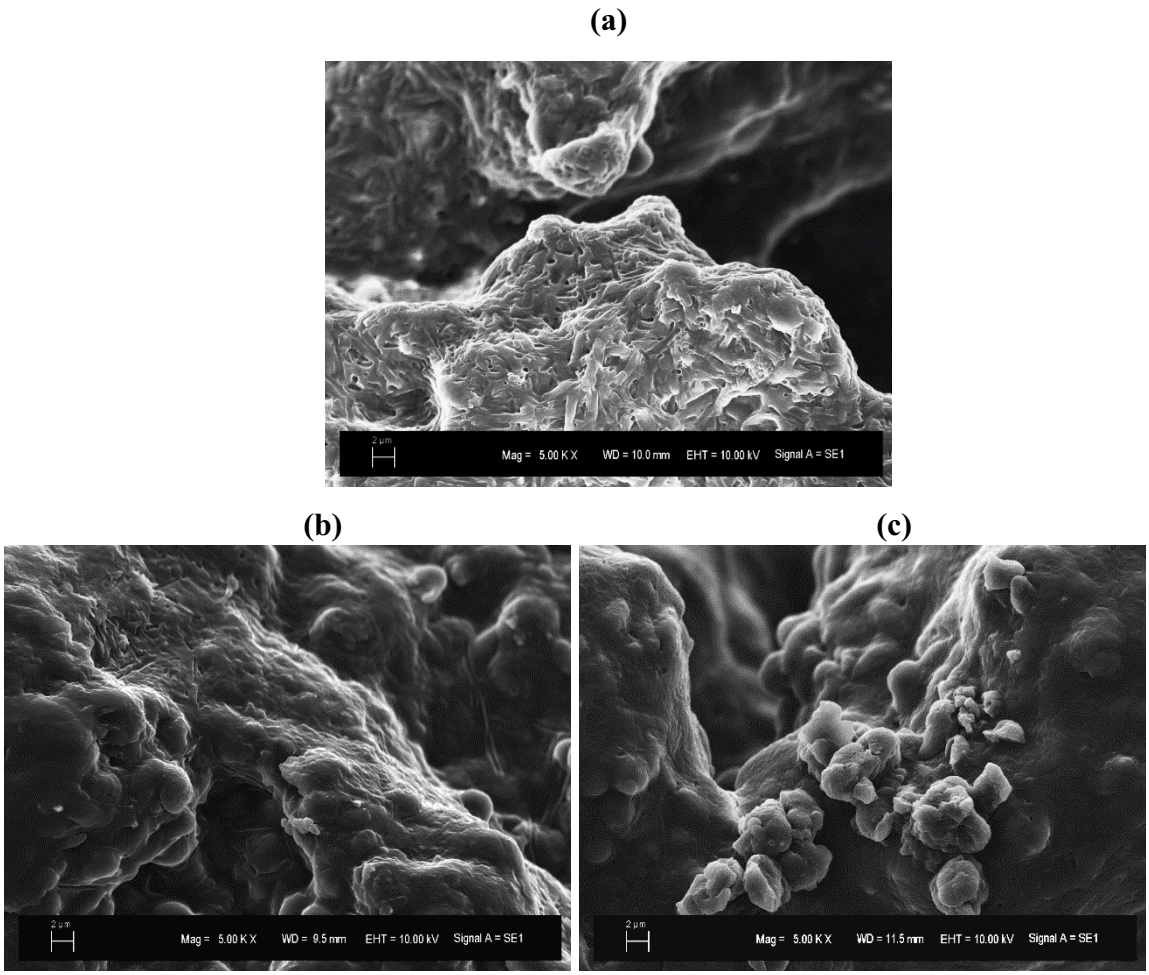

Fig. 1. SEM pictures of kefir biomass before (a) and after ultrasound-assisted (b) and conventional (c) bioaccumulation processes.

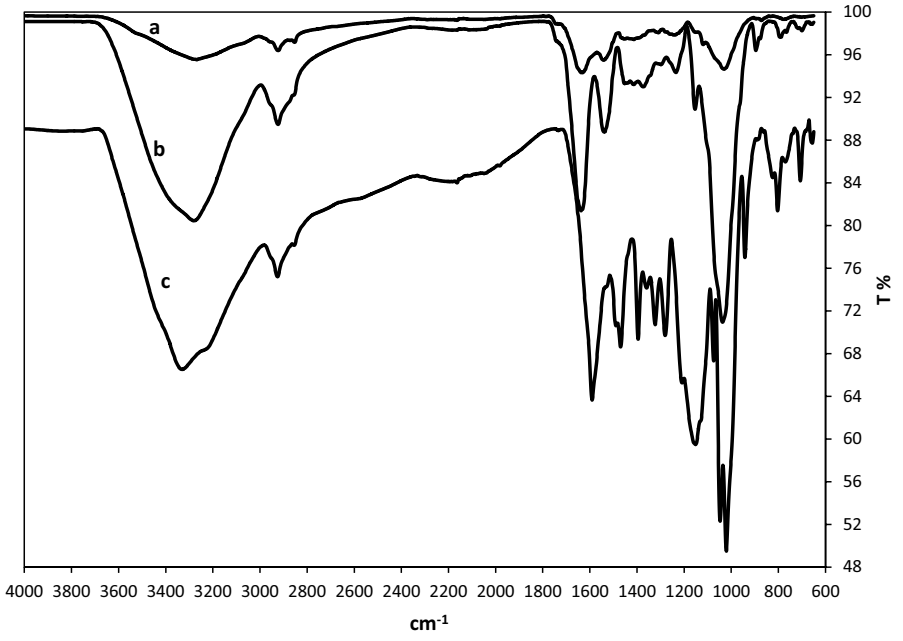

Fig. 2. FTIR spectra for: (a) kefir biomass before bioaccumulation, (b) IB dye, and (c) kefir biomass after bioaccumulation.

Table 2
Surface area and porosity of kefir biomass

	Brunauer–Emmett–Teller area ($m^2\ g^{-1}$)	Average pore diameter (BJH) (nm)		Cumulative pore volume (BJH) ($cm^3\ g^{-1}$)	
		Adsorption	Desorption	Adsorption	Desorption
Untreated biomass	2.79	3.16	3.067	5.46×10^{-3}	4.85×10^{-3}
Ultrasound treated biomass	2.97	3.16	3.42	4.66×10^{-3}	3.75×10^{-3}

Table 3
Minimum values of the determination coefficients for the kinetic models

Kinetic model	Ultrasound-assisted bioaccumulation	Conventional bioaccumulation
Pseudo-first-order	$R^2 > 0.97$	$R^2 > 0.98$
Pseudo-second-order	$R^2 > 0.99$	$R^2 > 0.90$
Intraparticle diffusion	$R^2 > 0.80$	$R^2 > 0.97$
Elovich	$R^2 > 0.83$	$R^2 > 0.96$

are shown in Figs. 3a and b and the related surface area and porosity information is given in Table 2. As seen in Table 2, the results obtained for the two samples do not differ significantly. The pore size distributions (Figs. 3a and b) show that the kefir biomass samples mainly contain mesopores (2.5 nm < pore diameter < 50 nm). In this study, the surface area measurements were conducted on oven-dried samples. kefir biomass shrinks when it is dried as about 90% of the content of biomass is water. Therefore, the actual values of the surface area and pore volume of the samples would be higher than the measured results.

3.2. Effect of initial pH

One of the most significant parameters in adsorption is the initial pH of the adsorbate solution as it can influence the ionisation degree of the adsorbate molecules, the surface charge of the adsorbent and the extent of decomposition of functional groups on the active zones of the adsorbent [28,29].

The effect of initial pH on ultrasound-assisted and conventional bioaccumulation of IB by kefir biomass was investigated for a pH range between 2 and 10, at 100 mg L^{-1} initial dye concentration and 25°C with the addition of 2.4 g L^{-1} kefir biomass. The results are illustrated in Fig. 4. Maximum dye removal percentages for ultrasonic-assisted and conventional processes were obtained at pH 2 as 82.1% and 41.4%, respectively. In both processes, dye removal decreased significantly with the increase in pH. This result is associated with the electrostatic interaction between the dye molecules and the biomass surface. As the PZC of kefir biomass is 4.46, the biomass surface is positively charged below pH 4.46 and negatively charged above pH 4.46. Accordingly, as the pH increases the number of protonated groups on the biomass surface decreases thus the attraction and adsorption of the anionic dye decreases.

With the ultrasound-assisted method, higher dye removal efficiencies were obtained at all pH values compared to the

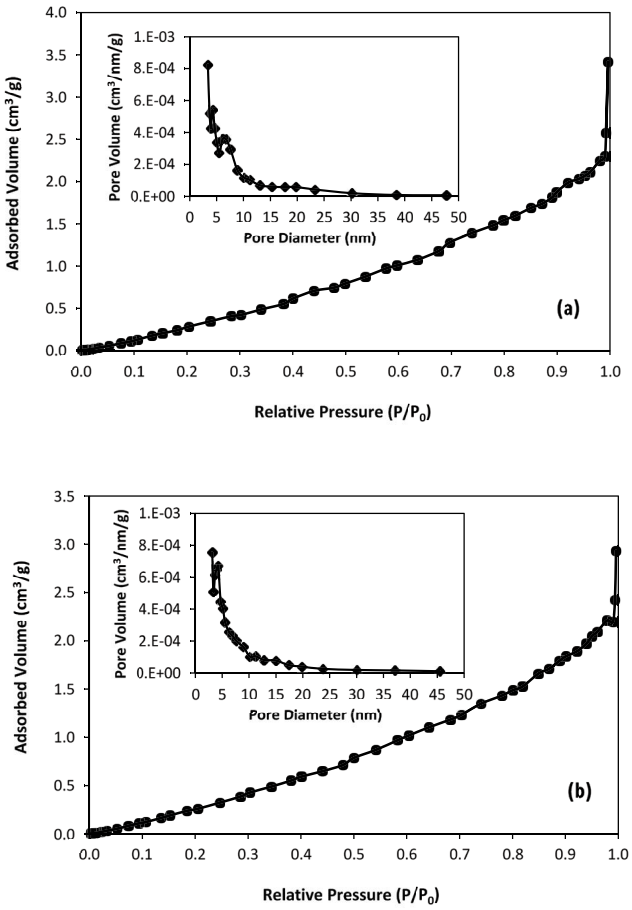

Fig. 3. Brunauer–Emmett–Teller surface area and pore size distribution analyses of (a) untreated kefir biomass and (b) ultrasound treated kefir biomass.

conventional method. However, as seen in Fig. 4, the enhancement effect of ultrasound is greater, especially at high pHs. The enhancement of bioaccumulation, considering the dye removal percentages in ultrasound-assisted and conventional processes, was 98% and 246% at pH 2 and pH 10, respectively.

Ultrasound has been applied simultaneously with adsorption to enhance the process efficiency in numerous works. Ultrasonic irradiation leads to acceleration in reaction and mass transfer rates because of acoustic cavitation. Cavitation covers the generation and subsequent growth and collapse of microbubbles leading to high energy densities and high local temperatures and pressures for a short time. Mass transfer in adsorption is limited by the diffusion-convection step in the process. The mass transfer

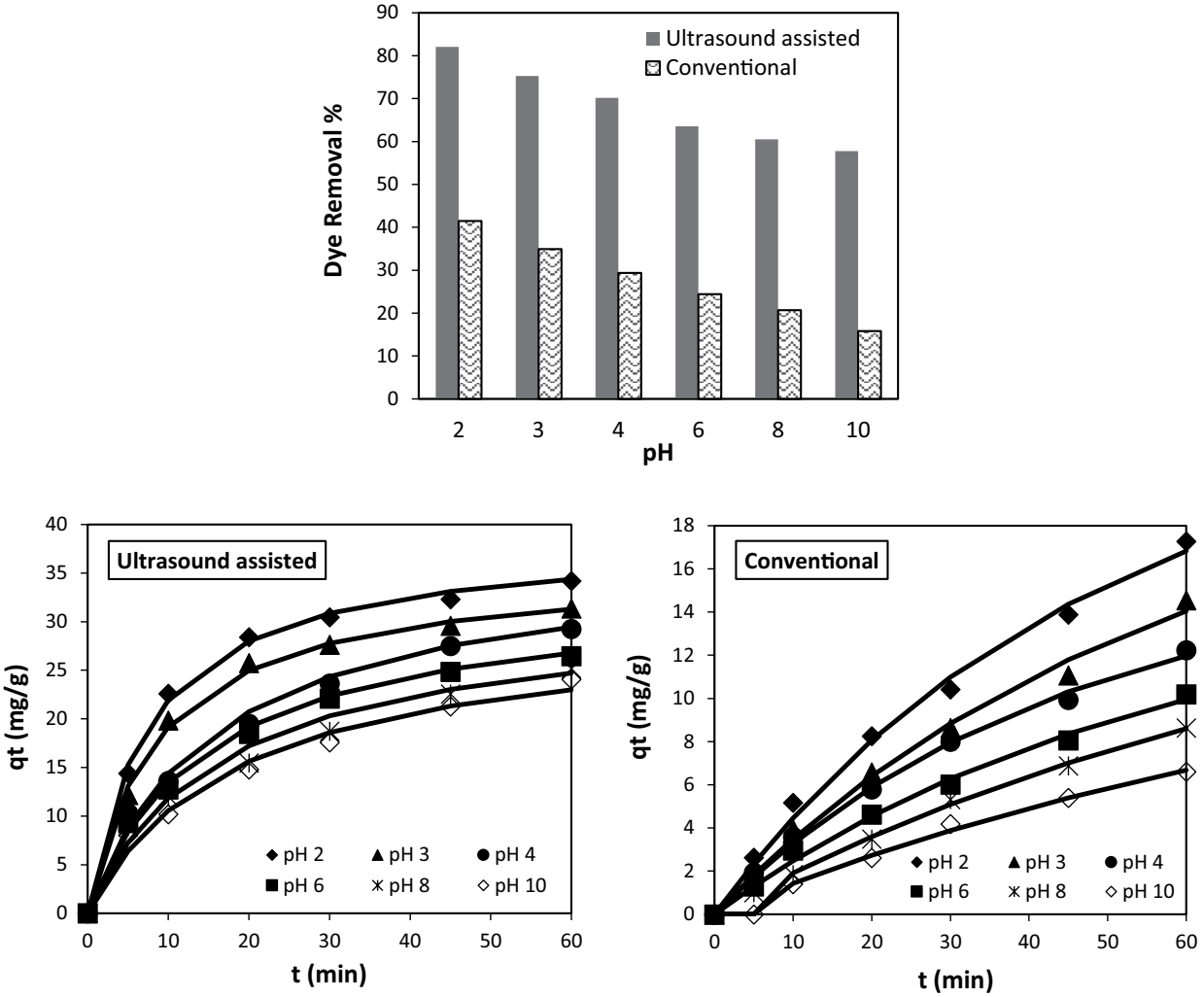

Fig. 4. The effect of initial pH on conventional and ultrasound-assisted bioaccumulation of IB by kefir biomass.

resistance can be eliminated by increasing the convection in the medium. Simply put, ultrasound power creates convection through acoustic waves [16–19]. Consequently, ultrasound-assisted adsorption compared to conventional adsorption processes could lead to faster equilibrium that significantly reduces the contact time. Also, it is recognised that low-frequency ultrasound is effective in enhancing cell membrane permeability [30,31]. In this study, the improvement in dye uptake with the assistance of ultrasound can be explained by the increase in cell membrane permeability and mass transfer rate because of sonic cavitation, bubble expansion and collapse, as well as shock waves and the thermal effects of ultrasound.

3.3. Effect of temperature

The effect of temperature on bioaccumulation processes was investigated in the range of 25°C–40°C at fixed initial pH (pH2), initial dye concentration (100 mg L^{-1}) and kefir grain dosage (2.4 g L^{-1}). The results are presented in Fig. 5.

The removal of IB dye increased with increasing temperatures in both processes, which indicates that the bioaccumulation processes are endothermic. When the temperature increased from 25°C to 40°C, the dye removal percentage and bioaccumulation capacity values increased from 82.1% to 98.9% and from 34.1 to 41.2 mg g^{-1}, respectively in the ultrasound-assisted process and from 41.4% to 80.5% and from 17.2 to 33.6 mg g^{-1}, respectively in the conventional process. At all temperatures, higher dye removal efficiencies were achieved with the ultrasound-assisted process compared to the conventional one. The results show that the difference between the efficiencies of the two processes increased as temperature decreased so indicating that the improvement and enhancement of the bioaccumulation by ultrasound is more significant especially at lower temperatures. With the assistance of ultrasound, the enhancement in bioaccumulation is 98% and 23% at 25°C and 40°C respectively. This improvement can be explained by the increase in cell membrane permeability and mass transfer rate as a result of the mechanical and thermal effects of ultrasound.

3.4. Effect of initial dye concentration

Initial adsorbate concentration is a significant parameter in adsorption since the concentration gradient acts as a driving force to overcome the resistance of mass transfer

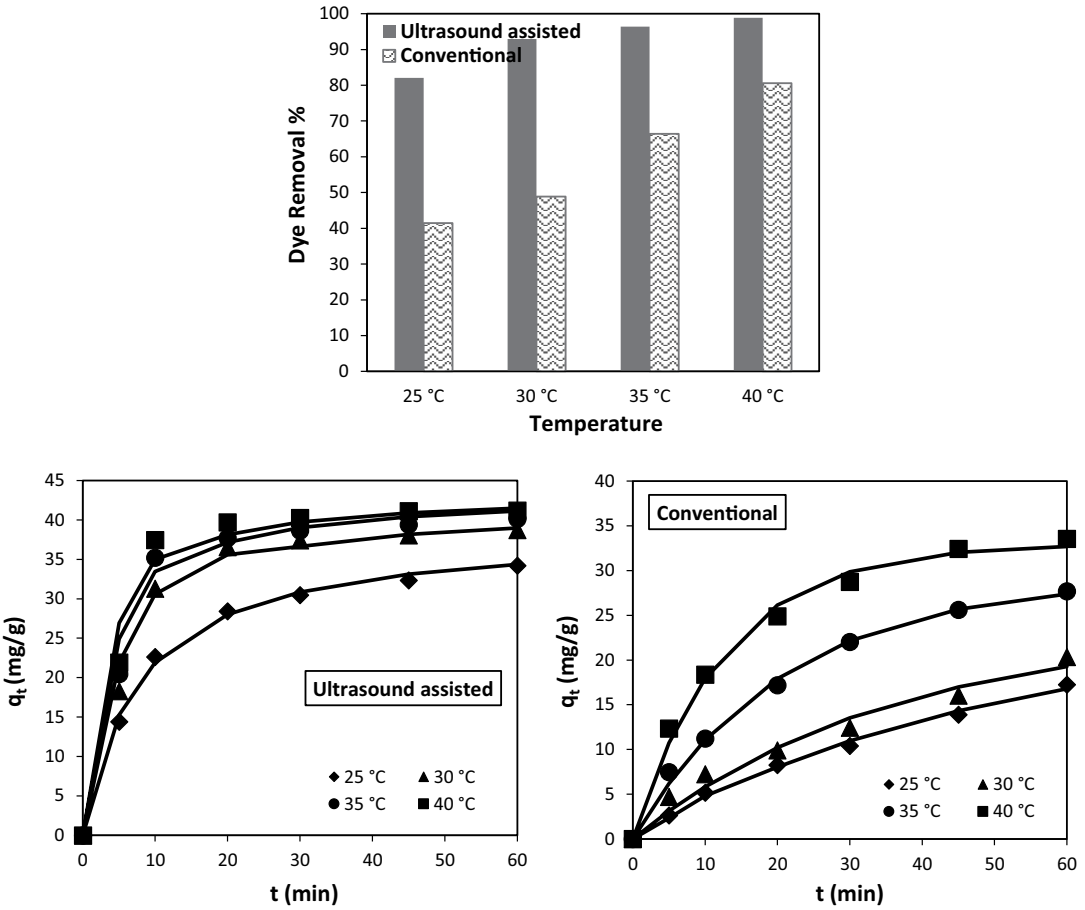

Fig. 5. The effect of temperature on conventional and ultrasound-assisted bioaccumulation of IB by kefir biomass.

between the liquid and solid phases in the diffusion of adsorbate molecules from solution to the adsorbent surface. The effect of initial dye concentration on ultrasound-assisted and conventional bioaccumulation of IB by kefir biomass was investigated in a 50–400 mg L^{-1} dye concentration range at pH 2 and 25°C with the addition of 2.4 g L^{-1} kefir biomass. The results are illustrated in Fig. 6.

Bioaccumulation capacities increased with the increase in initial dye concentration while dye removal percentages decreased. In 240 min processing times the maximum bioaccumulation capacity was achieved at 400 mg L^{-1} dye concentration as 107.4 mg g^{-1} for ultrasound-assisted bioaccumulation and 52.3 mg g^{-1} for the conventional bioaccumulation process. At high dye concentrations, the dye removal percentage decreases due to nearly all the binding sites on the biomass surface being filled. Conversely, at low dye concentrations, the dye removal percentage is high due to the free binding sites on the biomass surface.

With the application of ultrasound, the higher removal efficiencies and decreasing processing times to reach equilibrium clearly show the enhancement effect of ultrasound on bioaccumulation. As seen in Fig. 6, the enhancement in bioaccumulation by ultrasound is especially noticeable at higher dye concentrations. With the assistance of ultrasound, the improvement of bioaccumulation is 32% and 106% at 50 and 400 mg L^{-1} initial dye concentrations, respectively.

3.5. Spectral analysis of decolourisation

The removal of dyes by living biomass may be due to bioaccumulation and/or biodegradation. In the case of bioaccumulation of dyes, the comparison of the main peaks obtained from UV-Vis spectral scanning of the dye solutions before and after treatment shows a decrease in proportion to each other. However, in the case of biodegradation, the major peaks decrease sharply or disappear, and new peaks may be observed due to new metabolites emerging after degradation [32]. UV-Vis spectral analysis of IB dye solutions before and after 60 min of bioaccumulation processes is shown in Fig. 7. As seen from the figure, the untreated IB dye solution has a main peak at 500 nm in the visible region. This peak is found to decrease gradually after the conventional and ultrasound-assisted methods. No new peak formation was observed. These results indicate that in both methods the removal of azo dye IB was mainly achieved by bioaccumulation.

3.6. Bioaccumulation kinetics

The kinetic data presented in Figs. 4–6 were analysed using pseudo-first-order [Eq. (3)], pseudo-second-order [Eq. (4)], intraparticle diffusion [Eq. (5)] and Elovich [Eq. (6)] kinetic models. All tested models showed good

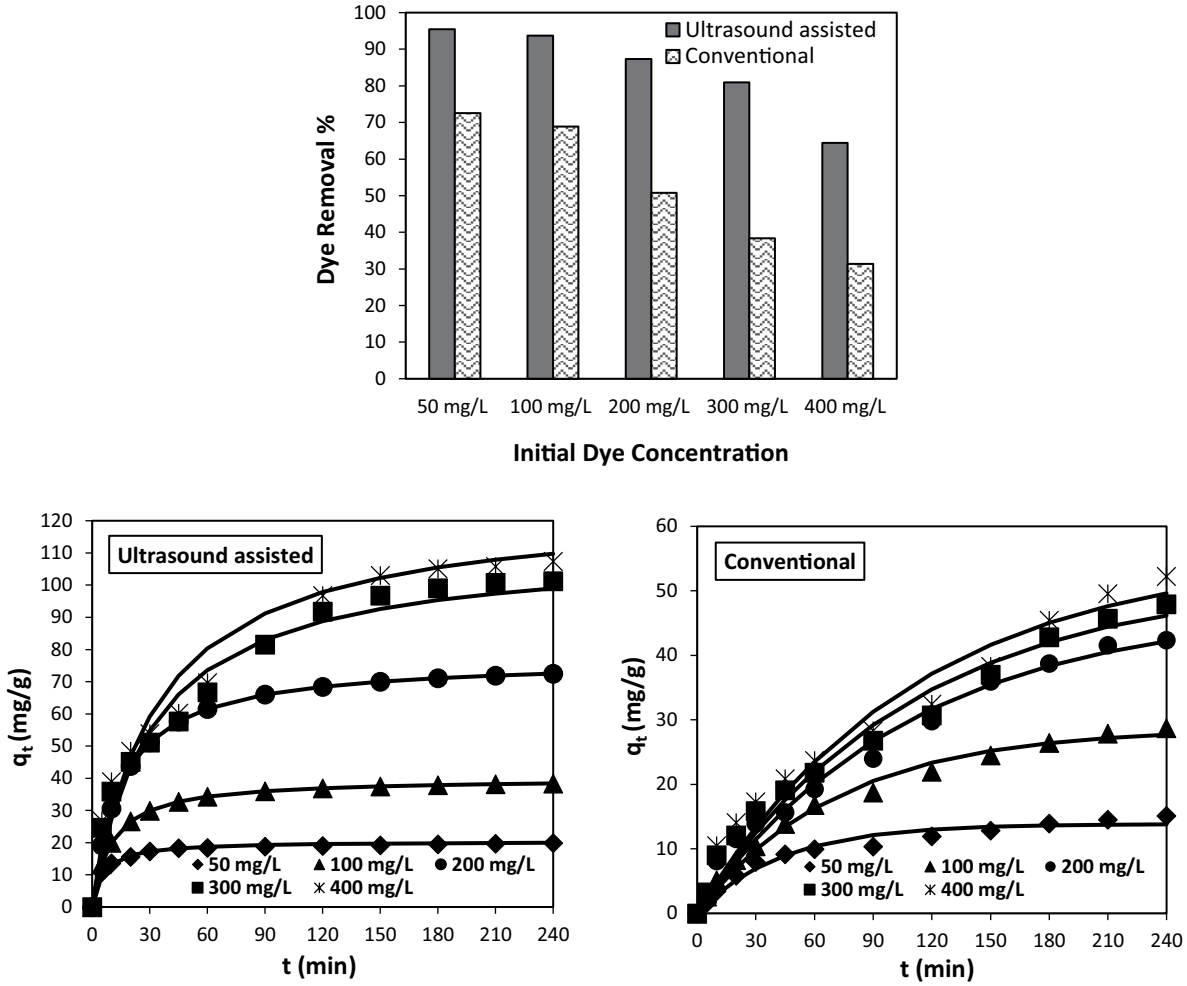

Fig. 6. The effect of initial dye concentration on conventional and ultrasound-assisted bioaccumulation of IB by kefir biomass.

compatibility with the experimental data. The minimum values of the determination coefficients for the models are summarised in Table 3.

Even though all models provided good fitness to experimental data, after evaluating all the data it was determined that the pseudo-second-order kinetic model provided the best fits to ultrasound-assisted bioaccumulation data, while the pseudo-first-order kinetic model provided the best fits to conventional bioaccumulation data. The constants and statistical data obtained for the pseudo-first and second-order kinetic models are given in Table 4. The fitness of the models is also shown in Figs. 4–6 (in the figures the solid lines represent the models).

Good fitness of more than one model to the experimental data indicates that the bioaccumulation of IB by kefir biomass is complex and may include several mechanisms. The good compatibility of the experimental data with the pseudo-first and pseudo-second-order kinetic models indicates that the occupation rate of sorption sites is proportional to the available active regions on the biomass surface. As compared to the other models, the low fitness of the experimental data to the intraparticle diffusion model and the determined *C* coefficients for the models that have non-zero values indicate that the intraparticle diffusion is not the rate-controlling step in bioaccumulation processes and the kinetics of bioaccumulation may be controlled by two or more mechanisms. On the other hand, the good fitness of the experimental data with the Elovich kinetic suggests that chemisorption may also be a controlling step in bioaccumulation processes.

3.7. Equilibrium modelling

Adsorption isotherms are employed to explain the interaction between adsorbate and adsorbent at equilibrium conditions, as well as the adsorption mechanism. In this study, the equilibrium data were evaluated with Freundlich, Langmuir and Temkin isotherm models. The obtained model constants and R^2 values are given in Table 5.

As seen in Table 5, all models displayed high conformity with equilibrium data. However, based on the values of coefficient of determination (R^2), it could be concluded that the adsorption isotherm of IB dye by kefir biomass is better defined by the Langmuir model than the Temkin and Freundlich models both for conventional and ultrasound-assisted bioaccumulation. The conformity of the Langmuir model to experimental data is shown graphically in Fig. 8.

Table 4
Constants and statistical data for the pseudo-first and second-order kinetic models

	Conventional bioaccumulation/ pseudo-first-order kinetic model				Ultrasound-assisted bioaccumulation/ pseudo-second-order kinetic model			
pH	k_1 (min^{-1})	q_e (mg g^{-1})	s	R^2	k_2 (g mg^{-1} min^{-1})	q_e (mg g^{-1})	s	R^2
pH 2	0.0211	23.44	0.52	0.99	0.0034	38.46	0.02	0.99
pH 3	0.0177	21.47	0.50	0.99	0.0032	35.71	0.02	0.99
pH 4	0.0230	15.99	0.27	0.99	0.0017	37.04	0.05	0.99
pH 6	0.0179	15.12	0.30	0.99	0.0020	33.33	0.04	0.99
pH 8	0.0124	16.39	0.13	0.99	0.0019	31.25	0.11	0.99
pH 10	0.0109	13.92	0.26	0.99	0.0017	30.30	0.12	0.99
Dye concentration								
50 mg L^{-1}	0.0232	13.85	0.91	0.98	0.0088	20.41	0.06	0.99
100 mg L^{-1}	0.0140	28.70	1.04	0.99	0.0025	39.99	0.06	0.99
200 mg L^{-1}	0.0092	47.33	2.10	0.99	0.0009	76.92	0.03	0.99
300 mg L^{-1}	0.0092	52.02	2.64	0.99	0.0003	111.1	0.07	0.99
400 mg L^{-1}	0.0091	55.92	3.40	0.98	0.0002	125.0	0.08	0.99
Temperature								
25°C	0.0211	23.44	0.52	0.99	0.0034	38.46	0.02	0.99
30°C	0.0285	23.53	1.26	0.99	0.0059	41.67	0.04	0.99
35°C	0.0482	28.98	0.67	0.99	0.0070	42.58	0.03	0.99
40°C	0.0787	32.98	1.15	0.99	0.0083	43.54	0.03	0.99

Table 5
Constants and statistical data for the isotherm models

Model		Ultrasound-assited bioaccumulation	Conventional bioaccumulation
Freundlich	K_F (mg g^{-1} (mg L^{-1})$^{-1/n}$)	22.15	4.63
	n	2.40	2.11
	s	0.16	0.24
	R^2	0.98	0.94
Langmuir	K_L (L mg^{-1})	0.24	0.012
	q_m (mg g^{-1})	102.25	86.51
	s	0.0034	0.0052
	R^2	0.99	0.99
Temkin	K_T (L mg^{-1})	1.80	0.19
	b_T (J mol^{-1})	100.83	165.12
	s	8.96	4.29
	R^2	0.98	0.98

The high compatibility of the Langmuir model with experimental data designates monolayer IB dye adsorption on homogeneous biomass surfaces. As can be seen from Table 5, the model revealed that the maximum bioaccumulation capacities are 86.5 and 102.3 mg g^{-1} for the conventional method and the ultrasound-assisted method, respectively. The good fitness of the Freundlich model to the experimental data displays multilayer heterogeneous adsorption sites. The sorption intensity (n) values of the model are within the range of 1–10 indicating favourable adsorption [33]. The good conformity of the Temkin model with experimental data suggests that the heat of adsorption of the molecules in the layer linearly decreases with coating. The b_T (heat of adsorption) values obtained from the model are 165 and 100 J mol^{-1} for conventional and ultrasound-assisted processes, suggesting that the uptake of IB dye in both processes was by physisorption [34].

4. Conclusion

Conventional and ultrasound-assisted bioaccumulation of direct azo dye Indosol Black NF-1200 by kefir biomass was investigated under different process conditions. The bioaccumulation of the dye was influenced by the pH of the solution, initial dye concentration and temperature. In all conditions with the assistance of ultrasound, higher

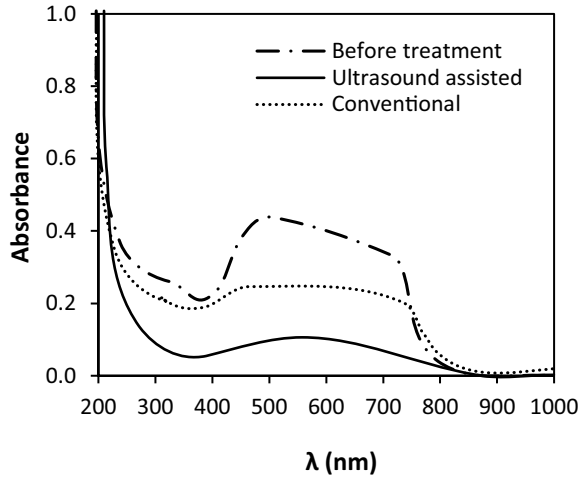

Fig. 7. UV-Vis spectral analysis of IB dye solutions.

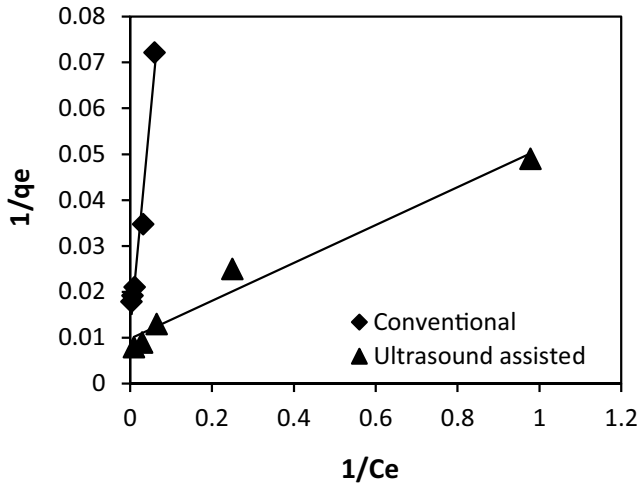

Fig. 8. The conformity of the Langmuir model to experimental data.

dye removal efficiencies were achieved, and the equilibrium times significantly decreased. However, the results show that the enhancement effect of ultrasound is more significant at high pHs, high dye concentrations and low temperatures. The kinetics of dye removal by ultrasound-assisted and conventional bioaccumulation were best described with pseudo-second-order and pseudo-first-order models, respectively. Equilibrium data were best described by the Langmuir isotherm model that gives maximum bioaccumulation capacities of 86.5 and 102.3 mg g^{-1} for the conventional and ultrasound-assisted methods. The results of this study demonstrate that the kefir biomass can be used effectively for the removal of direct azo dyes, and ultrasound is a powerful option for the improvement of bioaccumulation processes.

Acknowledgements

This work was supported by Research Fund of the Yildiz Technical University (FBA-2019–3709).

Symbols

b_T — Temkin isotherm constant related to the heat of adsorption, J mol^{-1}
C — Intraparticle diffusion model constant, mg g^{-1}
C_e — Equilibrium dye concentration, mg L^{-1}
C_0 — Initial dye concentration, mg L^{-1}
C_t — Dye concentrations at processing time t, mg L^{-1}
k_1 — Pseudo-first-order rate constant, min^{-1}
k_2 — Pseudo-second-order rate constant, g mg^{-1} min^{-1}
k_p — Intraparticle diffusion rate constant, mg g^{-1} $min^{-1/2}$
K_F — Freundlich constant, mg g^{-1} (mg $L^{-1})^{-1/n}$
K_L — Langmuir constant, L mg^{-1}
K_T — Temkin constant, L mg^{-1}
n^{-1} — Freundlich constant related to adsorption intensity, –
M — Kefir biomass weight, g
q_e — Adsorbed dye amount per unit mass of kefir biomass at equilibrium, mg g^{-1}
q_m — Maximum adsorption capacity, mg g^{-1}
q_t — Adsorbed dye amount per unit mass of kefir biomass at time t, mg g^{-1}
R — Universal gas constant, J mol^{-1} K^{-1}
R^2 — Coefficient of determination, –
s — Standard error, –
t — Time, min
T — Temperature, K
V — Volume, L

Greek symbols

α — Initial adsorption rate, mg g^{-1} min^{-1}
β — Desorption constant, g mg^{-1}

References

[1] M.T. Yagub, T.K. Sen, S. Afroze, H.M. Ang, Dye and its removal from aqueous solution by adsorption: a review, Adv. Colloid Interface Sci., 209 (2014) 172–184.
[2] F.M. Drumond Chequer, G.A. Rodrigues de Oliveira, E.R. Anastácio Ferraz, J. Carvalho Cardoso, M.V. Boldrin Zanoni, D. Palma de Oliveira, Eco-Friendly Textile Dyeing and Finishing, M. Gunay, Ed., Intech Open Limited, London, 2013, pp. 151–176.
[3] Y. An, H.L. Zheng, Q. Sun, X.Y. Zheng, Q.Z. Wu, R. Zhao, A novel floating adsorbents system of acid orange 7 removal: polymer grafting effect, Sep. Purif. Technol., 227 (2019) 115677, doi: 10.1016/j.seppur.2019.115677.
[4] B. Lellis, C.Z. Fávaro-Polonio, J.A. Pamphile, J.C. Polonio, Effects of textile dyes on health and the environment and bioremediation potential of living organisms, Biotechnol. Res. Innovation, 3 (2019) 275–290.
[5] M.R. Islam, M.G. Mostafa, Textile dyeing effluents and environment concerns – a review, J. Environ. Sci. Nat. Resour., 11 (2018) 131–144.
[6] I. Ali, Z.A. Alothman, A. Alwarthan, Uptake of propranolol on ionic liquid iron nanocomposite adsorbent: kinetic, thermodynamics and mechanism of adsorption, J. Mol. Liq., 236 (2017) 205–213.
[7] A. Esmaeli, M. Jokar, M. Kousha, E. Daneshvar, H. Zilouei, K. Karimi, Acidic dye wastewater treatment onto a marine macroalga, *Nizamuddina zanardini* (Phylum: Ochrophyta), Chem. Eng. J., 217 (2013) 329–336.
[8] J.Q. Zhu, J.Y. Li, Y.Y. Li, J. Guo, X. Yu, L. Peng, B.P. Han, Y. Zhu, Y.M. Zhang, Adsorption of phosphate and photodegradation of cationic dyes with BiOI in phosphate-cationic dye binary system, Sep. Purif. Technol., 223 (2019) 196–202.
[9] F.J. Cervantes, A.B. Dos Santos, Reduction of azo dyes by anaerobic bacteria: microbiological and biochemical aspects, Rev. Environ. Sci. Biotechnol., 10 (2011) 125–137.

[10] A. Esmaeili, M. Kalantari, Bioremoval of an azo textile dye, Reactive Red 198, by *Aspergillus flavus*, World J. Microbiol. Biotechnol., 8 (2012) 1125–1131.
[11] P.A. Joshi, S. Jaybhaye, K. Mhatre, Biodegradation of dyes using consortium of bacterial strains isolated from textile effluent, Eur. J. Exp. Biol., 5 (2015) 36–40.
[12] S.S. Phugare, D.C. Kalyani, A.V. Patil, J.P. Jadav, Textile dye degradation by bacterial consortium and subsequent toxicological analysis of dye and dye metabolites using cytotoxicity, genotoxicity and oxidative stress studies, J. Hazard. Mater., 186 (2011) 713–723.
[13] B. Gezer, Cu(II) adsorption with activated carbon obtained from sea urchin prepared by ultrasound-assisted method, NOHU J. Eng. Sci., 9 (2020) 770–780.
[14] S.K. Low, M.C. Tan, Dye adsorption characteristic of ultrasound pre-treated pomelo peel, J. Environ. Chem. Eng., 6 (2018) 3502–3509.
[15] G.L. Dotto, J.M.N. Santos, I.L. Rodrigues, R. Rosa, F.A. Pavan, E.C. Lima, Adsorption of Methylene Blue by ultrasonic surface modified chitin, J. Colloid Interface Sci., 446 (2015) 133–140.
[16] A. Asfaram, M. Ghaedi, S. Hajati, A. Goudarzi, E.A. Dil, Screening and optimization of highly effective ultrasound-assisted simultaneous adsorption of cationic dyes onto Mn-doped Fe_3O_4-nanoparticle-loaded activated carbon, Ultrason. Sonochem., 34 (2017) 1–12.
[17] V.R. Midathana, V.S. Moholkar, Mechanistic studies in ultrasound-assisted adsorption for removal of aromatic pollutants, Ind. Eng. Chem. Res., 48 (2009) 7368–7377.
[18] A.M. Ealias, M.P. Saravanakumar, A critical review on ultrasonic-assisted dye adsorption: mass transfer, half-life and half-capacity concentration approach with future industrial perspectives, Crit. Rev. Env. Sci. Technol., 49 (2019) 1959–2015.
[19] W.K. Zhang, Y. Liang, J.W. Wang, Y.R. Zhang, Z.Y. Gao, Y.Q. Yang, K. Yang, Ultrasound-assisted adsorption of Congo red from aqueous solution using Mg–Al–CO_3 layered double hydroxide, Appl. Clay Sci., 174 (2019) 100–109.
[20] D.K. Apar, E. Demirhan, B. Özel, B. Özbek, Kefir grain biomass production: influence of different culturing conditions and examination of growth kinetic models, J. Food Process. Eng., 40 (2017) e12332, doi: 10.1111/jfpe.12332.
[21] A.M. de Oliveira Leite, M.A.L. Miguel, R.S. Peixoto, A.S. Rosado, J.T. Silva, V.M.F. Paschoalin, Microbiological, technological and therapeutic properties of kefir: a natural probiotic beverage, Braz. J. Microbiol., 44 (2013) 341–349.
[22] A.O. Erdoğdular, D.K. Apar, Bioremoval of reactive dye Remazol Navy by kefir grains, Appl. Biol. Chem., 62 (2019) 22, doi: 10.1186/s13765-019-0429-1.
[23] A. Jenab, R. Roghanian, G. Emtiazi, K. Ghaedi, Manufacturing and structural analysis of antimicrobial kefiran/polyethylene oxide nanofibers for food packaging, Iran. Polym. J., 26 (2017) 31–39.
[24] Z. Chen, J.L. Shi, X.J. Yang, B. Nan, Y. Liu, Z.F. Wang, Chemical and physical characteristics and antioxidant activities of the exopolysaccharide produced by Tibetan kefir grains during milk fermentation, Int. Dairy J., 43 (2015) 15–21.
[25] H. Radhouani, C. Gonçalves, F.R. Maia, J.M. Oliveira, R.L. Reis, Kefiran biopolymer: evaluation of its physicochemical and biological properties, J. Bioact. Compat. Polym., 33 (2018) 461–478.
[26] A. Bartošová, L. Blinová, M. Sirotiak, A. Michalíková, Usage of FTIR-ATR as non-destructive analysis of selected toxic dyes, Res. Pap. Fac. Mater. Sci. Technol. Slovak Univ. Technol., 25 (2017) 103–111.
[27] A. Das, S. Mishra, Removal of textile dye reactive green-19 using bacterial consortium: process optimization using response surface methodology and kinetics study, J. Environ. Chem. Eng., 5 (2017) 612–627.
[28] H.M.H. Gad, A. El-Hakim, A.M. Daifullah, Impact of surface chemistry on the removal of indigo carmine dye using apricot stone active carbon, Adsorpt. Sci. Technol., 25 (2007) 327–341.
[29] X.S. Wang, Y. Zhou, Y. Jiang, Removal of methylene blue from aqueous solution by non-living biomass of marine algae and freshwater macrophyte, Adsorpt. Sci. Technol., 26 (2009) 853–863.
[30] J. Sundaram, B.R. Mellein, S. Mitragotri, An experimental and theoretical analysis of ultrasound-induced permeabilization of cell membranes, Biophys. J., 84 (2003) 3087–3101.
[31] C.H. Dai, F. Xiong, R.H. He, W.W. Zhang, H. Ma, Effects of low-intensity ultrasound on the growth, cell membrane permeability and ethanol tolerance of *Saccharomyces cerevisiae*, Ultrason. Sonochem., 36 (2017) 191–197.
[32] E. Zabłocka-Godlewska, W. Przystaś, Fed-batch decolourization of mixture of brilliant green and evans blue by bacteria species applied as pure and mixed cultures: influence of growth conditions, Water Air Soil Pollut., 231 (2020) 1–23.
[33] E. Ajenifuja, J.A. Ajao, E.O.B. Ajayi, Adsorption isotherm studies of Cu(II) and Co(II) in high concentration aqueous solutions on photocatalytically modified diatomaceous ceramic adsorbents, Appl. Water Sci., 7 (2017) 3793–3801.
[34] S. Sawasdee, P. Watcharabundit, Equilibrium, kinetics and thermodynamic of dye adsorption by low cost adsorbents, Int. J. Chem. Eng. Appl., 6 (2015) 444–449.